




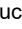
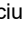







RESEARCH ARTICLE | MARCH 26 2024

Low temperature sputtering deposition of $Al_{1-x}Sc_xN$ thin films: Physical, chemical, and piezoelectric properties evolution by tuning the nitrogen flux in $(Ar + N_2)$ reactive atmosphere

M. A. Signore ; A. Serra ; D. Manno ; G. Quarta ; L. Calcagnile ; L. Maruccio ; E. Sciurti ; E. Melissano ; A. Campa; M. C. Martucci ; L. Francioso ; L. Velardi  



J. Appl. Phys. 135, 125105 (2024)

<https://doi.org/10.1063/5.0202683>



Articles You May Be Interested In

Identifying and overcoming the interface originating c-axis instability in highly Sc enhanced AlN for piezoelectric micro-electromechanical systems

J. Appl. Phys. (July 2017)

Stress controlled pulsed direct current co-sputtered $Al_{1-x}Sc_xN$ as piezoelectric phase for micromechanical sensor applications

APL Mater. (November 2015)

Preparation and performance of AlSc alloy targets

AIP Conference Proceedings (March 2022)



Journal of Applied Physics

Special Topics Open for Submissions

[Learn More](#)

Low temperature sputtering deposition of $\text{Al}_{1-x}\text{Sc}_x\text{N}$ thin films: Physical, chemical, and piezoelectric properties evolution by tuning the nitrogen flux in $(\text{Ar} + \text{N}_2)$ reactive atmosphere

Cite as: J. Appl. Phys. 135, 125105 (2024); doi: 10.1063/5.0202683

Submitted: 6 February 2024 · Accepted: 9 March 2024 ·

Published Online: 26 March 2024



View Online



Export Citation



CrossMark

M. A. Signore,¹ A. Serra,^{2,3} D. Manno,^{2,3} G. Quarta,^{2,3} L. Calcagnile,^{2,3} L. Maruccio,^{2,3} E. Sciurti,¹ E. Melissano,¹ A. Campa,¹ M. C. Martucci,¹ L. Francioso,¹ and L. Velardi^{1,a)}

AFFILIATIONS

¹CNR-IMM, Institute for Microelectronics and Microsystems, Via Monteroni, 73100 Lecce, Italy

²Department of Mathematics and Physics, CEDAD—Centre of Applied Physics Dating and Diagnostics, University of Salento, Via Monteroni, 73100 Lecce, Italy

³INFN Section of Lecce, Via Monteroni, 73100 Lecce, Italy

^{a)}Author to whom correspondence should be addressed: luciano.velardi@cnr.it

ABSTRACT

This work investigates the physical properties of $\text{Al}_{1-x}\text{Sc}_x\text{N}$ thin films sputtered at low temperatures by varying the process conditions. Specifically, the films were deposited at room temperature by applying a radio frequency power equal to 150 W to an AlSc alloy (60:40) target, varying the nitrogen flux percentage in the $(\text{Ar} + \text{N}_2)$ sputtering atmosphere (30%, 40%, 50%, and 60%) and keeping constant the working pressure at 5×10^{-3} mbar. The structural and chemical properties of the $\text{Al}_{1-x}\text{Sc}_x\text{N}$ films were studied by x-ray diffraction and Rutherford backscattering spectrometry techniques, respectively. The piezoelectric response was investigated by piezoresponse force microscopy. In addition, the surface potential was evaluated for the first time for Sc-doped AlN thin films by Kelvin probe force microscopy, providing piezoelectric coefficients free from the no-piezoelectric additional effect to the mechanical deformation, i.e., the electrostatic force. By alloying AlN with scandium, the piezoelectric response was strongly enhanced (up to 200% compared to undoped AlN), despite the low deposition temperature and the absence of any other additional energy source supplied to the adatoms during thin film growth, which generally promotes a better structural arrangement of polycrystalline film. This is a strategic result in the field of microelectromechanical systems completely fabricated at low temperatures.

© 2024 Author(s). All article content, except where otherwise noted, is licensed under a Creative Commons Attribution (CC BY) license (<https://creativecommons.org/licenses/by/4.0/>). <https://doi.org/10.1063/5.0202683>

I. INTRODUCTION

Piezoelectric thin films represent an indispensable building block in microelectromechanical systems (MEMS), which find application in many fields, spanning from telecommunication to energy harvesters or biomedical devices.^{1–3} AlN is one of the most studied piezoelectric materials for MEMS thanks to many advantages coming from its extraordinary physical and chemical properties together with the compatibility of the growth process with standard CMOS technology.^{4,5} A drawback of AlN is its low piezoelectric response as compared to more conventional materials such

as lead zirconate titanate (PZT), limiting its effective integration into piezoelectric devices.

One possible approach to improve the piezoelectric response of AlN thin films is to alloy the binary compound.⁶ To this aim, AlN doping with scandium (Sc) represents a potential way for high-performance piezoelectric films.^{7,8} The synthesis of crystal wurtzite $\text{Al}_{1-x}\text{Sc}_x\text{N}$ alloys⁹ is a great and recent challenge in the scientific community since it is not easy to achieve.

Sputtering is the most widely used technique to realize $\text{Al}_{1-x}\text{Sc}_x\text{N}$ films of good structural quality,^{10–16} due to lower

process complexity such as lower deposition temperature compared to other techniques.^{17–20} It is known that high substrate temperature promotes the films' densification through the diffusion of the incident species on the surfaces as also the improvement of morphological, optical, and electrical properties of the films.²¹ On the other hand, low substrate temperatures have important advantages from a technological point of view, considering that not all substrates can withstand high temperatures as also that low substrate temperatures could favor the device fabrication that monolithically integrates AlN-based thin films with temperature-sensitive materials.²²

In 2009, Akiyama *et al.*²³ reported the AlScN solid solution films deposited at 580 °C on Si(100) substrates using a dual radio frequency (RF) magnetron reactive co-sputtering, in which only the wurtzite phase was observed for the Sc contents less than 0.41 with a remarkable degradation of the structure quality for Al_{0.67}Sc_{0.33}N film. In the wurtzite structure, they evaluated an increase of the piezoelectric response equal to 400% compared to the AlN film.

The piezoelectric characterization of Al_{1-x}Sc_xN thin films reported in the literature is mainly performed by the Berlincourt method^{24–26} demonstrating that when Sc concentration in the AlN matrix exceeds the value of 50%, the piezoelectric properties get lost.^{12,27} In Ref. 23, the most intense piezoelectric response is obtained when the Sc concentration is equal to 42%. On the contrary, few works are reported in the literature about piezoresponse force microscopy (PFM) characterization of Al_{1-x}Sc_xN thin films. In Ref. 19, the ternary films deposited on GaN substrates by MBE exhibit a d_{33} value equal to 15 pm/V when $x = 0.18$, with a 150% enhancement in the piezoelectric coefficient compared to the AlN film (6 pm/V). Sc concentration higher than 0.18 causes a decrease of the piezoelectric coefficient attributed to a worsening in the crystalline quality. For Sc composition near 0.18, the literature reports d_{33} values of 5,²⁸ 7,²⁹ and 14 pm/V.³⁰ It is remarkable to highlight that d_{33} values reported from the literature for Al_{1-x}Sc_xN thin films and obtained by the PFM measurement have never been corrected from no-piezoelectric additional signals such as electrostatic contribution.

The aim of this work is to study the chemical, structural, and piezoelectric properties of sputtered Al_{1-x}Sc_xN thin films by using an AlSc alloy target, by tuning the nitrogen flux percentage in the (Ar + N₂) reactive process atmosphere. In addition, through the evaluation of the surface potential by Kelvin Probe Force Microscopy (KPFM), this investigation provides for the first time the piezoelectric coefficient of this new ternary material free from the no-piezoelectric additional effect to the mechanical deformation, i.e., the electrostatic force. All depositions were conducted at low temperatures, making easier and compatible the integration of the piezoelectric thin films in microelectromechanical systems

(MEMS) fabrication based on CMOS technology. It could be argued that high temperatures favor a more ordered structural arrangement of thin films but at the same time, they often limit the material choices in MEMS structures.³¹

II. EXPERIMENTAL DETAILS

Al_{1-x}Sc_xN thin films were deposited by RF magnetron sputtering technique using AlSc alloy (60:40) target (4 in, in size) known for its advantages in terms of deposition rate, industrial scalability, and constant Sc content across large substrates compared to the process using two mono-elemental targets.³² All films were deposited on 200 nm-thick titanium seed layer, sputtered on Si (100) substrate (size 15 × 15 mm²). Before the depositions, the chamber was evacuated down to 5 × 10⁻⁷ mbar. The deposition processes were conducted at room temperature, at a pressure equal to 5 × 10⁻³ mbar and RF power applied to target equal to 150 W. The maximum temperature reached during the sputtering deposition was 55 °C (measured by thermocouple). The target-substrate distance was 11 cm. Nitrogen flux percentage $P_{N_2} = \frac{\Phi_{N_2}}{\Phi_{(N_2+Ar)}} \times 100$ in the sputtering atmosphere was the tuned parameter, keeping constant the total gas flow (20 sccm). P_{N_2} was fixed at four values, 30%, 40%, 50%, and 60% in order to study its influence on the physical properties of the nitride films. The films were labeled according to the nitrogen percentage as AlScN_30, AlScN_40, AlScN_50, and AlScN_60. Their thickness, evaluated by profilometer (KLA Tenkor-P7), varies from 800 to 1300 nm (see Table I).

The elemental composition of the films was investigated by the Rutherford Backscattering Spectrometry (RBS) technique. RBS analyses were carried out at the CEDAD-Centre of Applied Physics, Dating and Diagnostics (University of Salento) by using a 3 MV Tandemron accelerator.³³ The ion beam (2 MeV He⁺⁺ ion beam, radius of 1 mm, current of 10–20 nA) was directed perpendicularly to the film surfaces. The RBS signals were recorded by a Canberra PIPS detector (active area of 25 mm², thickness of 300 μm, and resolution of 18 keV) positioned at an angle of 170° with the incident normal to the sample. The spectra were analyzed by SIMNRA software, which enabled the stoichiometric composition of the films and their thickness to be determined.

The crystalline structure and crystal orientation of Al_{1-x}Sc_xN films were analyzed by x-ray diffraction (XRD, Rigaku Miniflex x-ray diffractometer) in Bragg–Brentano geometry by using the Cu-Kα radiation and scanning angle of 2θ = 10°–80°. The spectra curves were fitted by a Voigt function to extract the full width at half maximum (FWHM) for crystal quality assessment. The mean crystallite size D normal to diffracting planes was evaluated by the Scherrer formula: $D = \frac{kl}{\beta \cos\theta}$ ³⁴ where K is the shape factor of the

TABLE I. Main characteristics of the analyzed thin films.

Sample label	$\Phi_{N_2}/(\Phi_{N_2} + \Phi_{Ar})$ (%)	Roughness, R_q (nm) by AFM	Thickness (nm) by profilometer	d_{33} (pm/V) by PFM
AlScN_30	30	8.0 ± 1.2	1340 ± 150	3.4 ± 0.6
AlScN_40	40	4.5 ± 0.1	975 ± 92	11.1 ± 1.9
AlScN_50	50	2.4 ± 0.2	820 ± 85	3.6 ± 0.4
AlScN_60	60	1.4 ± 0.1	775 ± 72	1.7 ± 0.1

average crystallite with a value of 0.9, λ is the x-ray wavelength (1.5405 Å for Cu target), β is the FWHM in radians, and θ is the Bragg angle.

Surface topography and morphology were analyzed by Atomic Force Microscopy (AFM) using a Nanosurf CoreAFM instrument. The same apparatus was also used for piezoresponse force microscopy (PFM) and Kelvin probe force microscopy (KPFM) measurements.

AFM topography 2D and 3D images were acquired over $2 \times 2 \mu\text{m}^2$ scan areas (resolution of 256×256 points) in non-contact mode, at room temperature, and in air environment. Silicon probe tips with diamond-like-carbon conductive coating (MULTI75E-G) were used at the typical resonance frequency of 75 kHz, with a constant force of 3 N/m.

Piezoelectric amplitude and phase, and sample topography signals were recorded simultaneously for PFM measurements, by scanning $0.5 \times 0.5 \mu\text{m}^2$ areas at ten different positions on the films' surface. First, periodically poled lithium niobate LiNbO₃ (PPLN) single-crystalline $500 \mu\text{m}$ -thick plate with roughness less than 10 nm, cut normal to the polar axis (PFM03- NT-MDT Spectrum Instruments), was used for system calibration to ensure 180° phase shift between inverted piezoelectric domains. An alternating excitation voltage of 10 V with a frequency of 20 kHz was applied through a Silicon probe tip with Cr/Pt conductive coating (MULTI75E-G, applied force equal to 20 nN) and the scans were performed in contact mode. The films were characterized by applying an alternating voltage V_{AC} in the range 1–5 V with a frequency of 3 kHz, very far from the tip resonance frequency (75 kHz). KPFM analyses were performed on $0.5 \times 0.5 \mu\text{m}^2$ areas at three different positions on the films' surface. During KPFM measurement, a V_{AC} voltage with an amplitude equal to 3 V and a frequency of 17 kHz were applied to a MULTI75E-G cantilever. Before measuring the samples, the work function of the probe was calibrated by using a sample test with Al and Au line arrays, and the work function of the tip was evaluated.

III. RESULTS AND DISCUSSION

A. Structural and chemical analyses of Al_{1-x}Sc_xN thin films

As already reported in Sec. II, the percentage of nitrogen reactive gas in the mixture [$\Phi_{N_2}/(\Phi_{N_2} + \Phi_{Ar})$] has been selected as a tuned parameter to vary the Sc content in the growing films and study the evolution of their physical properties. As expected, the deposition rate decreases with nitrogen flux percentage increasing in the sputtering mixture, as depicted in Fig. 1.³⁵

Taking into account the ions species available in the plasma, the more massive Ar⁺ ions have a higher sputtering yield than N⁺ and N²⁺ and they increase the deposition rate when predominant in the sputtering mixture (nitrogen percentage equal to 30% and 40%). At the same time, target poisoning increases with rising nitrogen content in the deposition chamber, as confirmed by the trend of the target bias voltage. As it can be observed from Fig. 1, the discharge voltage decreases with N₂ percentage rising, indicating a transition from metal to poisoned target (nitridation), characterized by an increase in the secondary electron emission coefficient confirmed by a discharge voltage decrease.³⁶

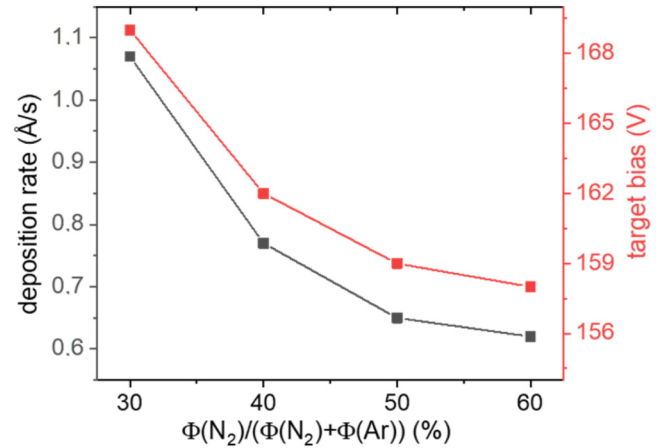


FIG. 1. Deposition rate and target bias voltage vs nitrogen flux percentage P_{N_2} in the sputtering reactive mixture.

The incorporation of Sc atoms into the AlN wurtzite structure was verified by non-destructive RBS analysis that provides elemental depth profiles of the samples. Figure 2 reports the RBS spectra of the investigated Al_{1-x}Sc_xN thin films varying reactive gas percentage in the chamber.

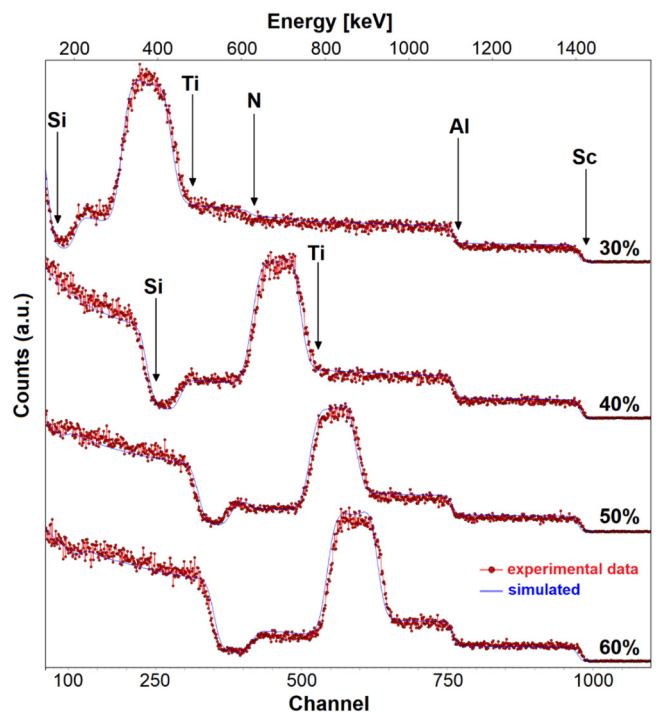


FIG. 2. RBS spectra of the analyzed Al_{1-x}Sc_xN thin films by varying P_{N_2} percentage in the sputtering reactive mixture.

TABLE II. Elemental composition of the analyzed films as found by RBS measurements (the associated error is 1%).

Sample	Al (%)	N (%)	Sc (%)	O (%)
AlScN_30	41	40	12	7
AlScN_40	39	41	16	4
AlScN_50	39	43	15	3
AlScN_60	42	44	9	5

All the spectra were analyzed by SIMNRA software; the red dots are the experimental data while the blue line represents the best fit obtained by entering Si, Ti, Al, Sc, N, and O elements in the software. The spectra show well-defined Sc and Al signal margins, indicating good film quality in terms of uniformity, low surface roughness, and good substrate–film interfaces.

The signal of the titanium seed layer is clearly visible for all the investigated films and its position is related to the film thickness. The nitrogen signal is visible only in the spectrum of AlScN_30 film, as it is not covered by the signal of Ti, which is positioned at low energy.

The signals coming from silicon (low energy part of the spectrum) are also visible and constitute the substrate, unlike the oxygen which is covered by the other signals. It should be noted that although the oxygen signal is not directly evident in the spectra, its presence and concentration were estimated indirectly by optimizing the fitting between the simulated and experimental spectra. In fact, simulations performed without oxygen were inaccurate.

The composition analysis calculated by using SIMNRA software is reported in Table II. It clearly indicates that scandium is incorporated in non-negligible amounts, from 9% to 16%, in accordance with what is reported in other papers.^{8–15} The thicknesses of the films, evaluated by SIMNRA software by considering for the ternary compounds a density equal to 3.28 g/cm³,³⁷ and calculated as an average value on three points around the center of the samples, belong to the same range found by profilometer measurements.

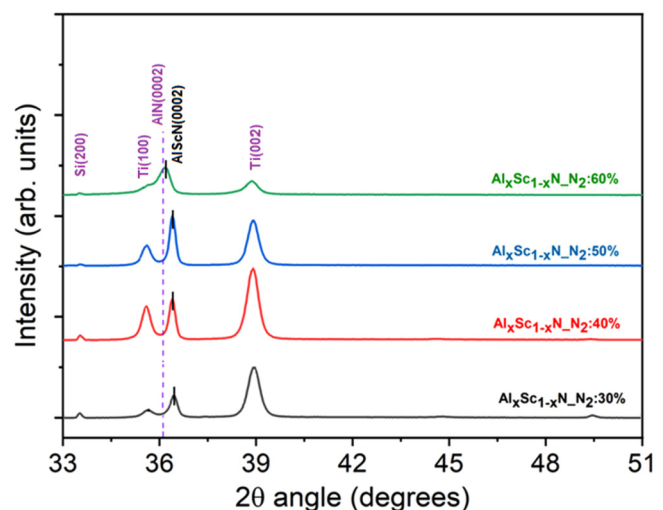
Furthermore, considering the RBS spectra and the elemental analyses reported in Table II, it can be deduced that:

- the increasing of nitrogen in the films is compatible with a higher N₂ concentration in the sputtering chamber available for the films' growth;
- the difference of scandium ratio between the film and the alloy target is due to differences in the single element sputtering yield, because the sputtering yield of scandium is lower than that of aluminum; moreover, it has been already reported in the literature the important role of target surface nitridation too, causing the reduction of the Sc content in the deposited films compared to the initial target composition;³⁸
- the detected oxygen content can be ascribed to different sources: the background contamination in the films, the silicon-titanium oxidated interface, and the oxidation of the films' surface after air exposure;

- the highest oxygen content is found in the film with a lower nitrogen content being O atoms substitutional of N ones; and
- the Sc/Al ratio and the composition between the films and target are different: several phenomena involved in the sputtering process, i.e., atoms re-evaporation and re-sputtering by backscattered neutral Ar, make challenging the control of the stoichiometry of the deposited films compared to alloyed target one.³⁹

Figure 3 shows the structural evolution of the Al_{1-x}Sc_xN thin films through the XRD spectra, by tuning the reactive gas percentage from 30% to 60%.

All nitride films show only the (002) diffraction peak of the wurtzite phase, besides Ti peaks used as a seed layer to promote the growth along *c* axis, advantageous for a more intense piezoelectric response. N₂ gas concentration in the sputtering mixture has a strong influence on the Al_{1-x}Sc_xN thin films crystalline quality, being closely related to the Sc content. It is evident from Fig. 3 that the 2θ₀₀₂ peak position of Al_{1-x}Sc_xN film moves toward higher angles from (002) peak position of wurtzite AlN peaked at 2θ = 36.03 (Card No. 25-1133) and indicated by a dashed line in the same figure, whatever the N₂ gas concentration in the sputtering mixture is. The substitution of Sc atoms into Al sites causes stress and distortion into the AlN crystal lattice which undergoes a tensile stress, as deducible from peak shift. This behavior has been already reported in the literature^{40–42} and it is ascribed to the Sc atoms insertion into the AlN wurtzite structure and to the different atomic radii of Al and Sc. The greatest peak shifts toward higher 2θ values are observed in the spectra of films with higher Sc content (AlScN_40 and AlScN_50), in agreement with RBS analysis. In addition, the peak shift also indicates a contraction in lattice spacing; specifically, the lattice is compressed. As a matter of fact, Sc atom insertion modifies the *c*-lattice parameter of pure w-AlN.

**FIG. 3.** XRD spectra of Al_{1-x}Sc_xN thin films sputtered by tuning the reactive gas flux percentage in the sputtering mixture.

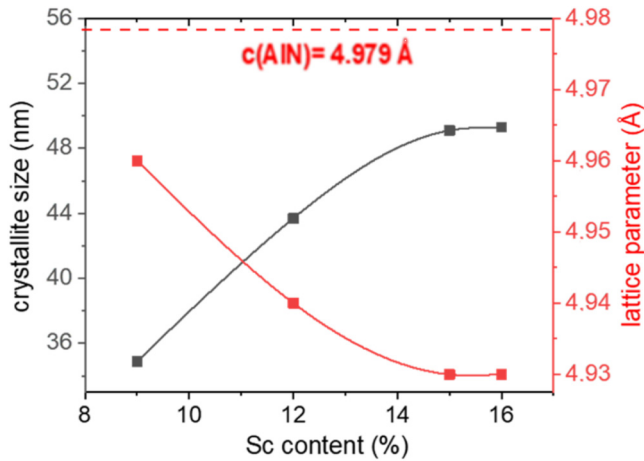


FIG. 4. Evolution of the c -lattice parameter and crystallite size of $\text{Al}_{1-x}\text{Sc}_x\text{N}$ thin films vs Sc content.

Reference c value for no stressed AlN thin film is 4.97 \AA (Card No. 25-1133). The corresponding lattice parameters for $\text{Al}_{1-x}\text{Sc}_x\text{N}$ thin films increasing N_2 percentage in the chamber from 30% to 60% are 4.94, 4.93, 4.93, and 4.96 \AA , respectively, as reported in Fig. 4,

TABLE III. Sc content (%) evaluated by RBS analysis and XRD data (Vegard's rule).

Sample	Sc content (%)	
	RBS	XRD
AlScN_30	12	10
AlScN_40	16	14
AlScN_50	15	14
AlScN_60	9	7

together with the crystallite size. They are comparable to values found by other authors, considering the range of Sc content in the ternary compounds detected in our work.^{43,44}

An opposite behavior in the crystallite size and c -lattice parameters is observed: an increase in the former correlates with a decrease in the latter and vice versa. The highest crystallite size is found for the sample with the highest Sc content incorporation (AlScN_40) where it reaches a value equal to 49.3 nm.

A theoretical approach to evaluate the Sc content in AlN films by exploiting XRD spectra can be made. The stoichiometry of the ternary compound $\text{Al}_{1-x}\text{Sc}_x\text{N}$ can be obtained by considering the wurtzite structure of AlN and ScN and applying Vegard's rule. This is based on the linear relationship between a -lattice parameter

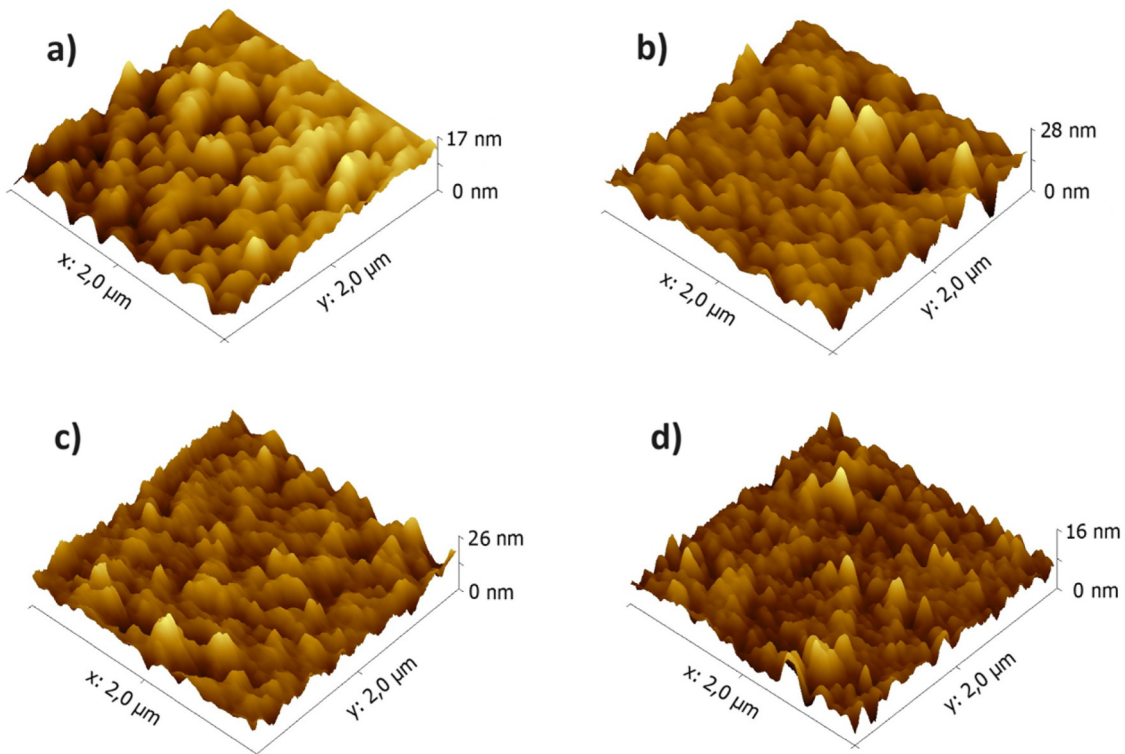


FIG. 5. AFM topography ($2 \times 2 \mu\text{m}^2$) of $\text{Al}_{1-x}\text{Sc}_x\text{N}$ thin films deposited at N_2 flux percentage of (a) 30%, (b) 40%, (c) 50%, and (d) 60%.

of the wurtzite structure and the stoichiometry of the ternary compound,

$$a(\text{Al}_{1-x}\text{Sc}_x\text{N}) = (1-x)a_{\text{AlN}} + xa_{\text{ScN}}. \quad (1)$$

To take into consideration a axis values (not deducible from our XRD spectra), an approximation could be done considering the work of Höglund *et al.*,⁴⁵ where the lattice parameters a and c for both nitrides in the wurtzite structure have been declared together with the c/a ratio in the ideal case. Starting from our experimental c values calculated from (002) XRD peak position of $\text{Al}_{1-x}\text{Sc}_x\text{N}$ films, the respective a value can be approximately evaluated from the theoretical $c/a = 1.602$ ratio reported in the above-mentioned work. The wurtzite ScN a parameter was declared equal to 3.47 Å,

obtained from a local minimum in the energy landscape by using a fixed $c/a = 1.6$ ratio. The substitution of these values into Vegard's relation (1) provides an approximated trend of the Sc atoms concentration in our films. The Sc content trend is consistent with RBS results, considering the approximations of the method, as can be observed in Table III.

The structural evolution in the $\text{Al}_{1-x}\text{Sc}_x\text{N}$ thin films, due to the Sc incorporation, obviously impacts the surface morphology, as observable by topographic AFM images reported in Fig. 5.

It is evident that the films where the Sc content is very close (AlN_40 and AlN_50) have a similar morphology [Figs. 5(b) and 5(c)]. Moreover, it was found that these two films have an average larger crystallite size (as deducible from the y -scales of the 3D AFM images), in contrast to the films deposited at 30% and

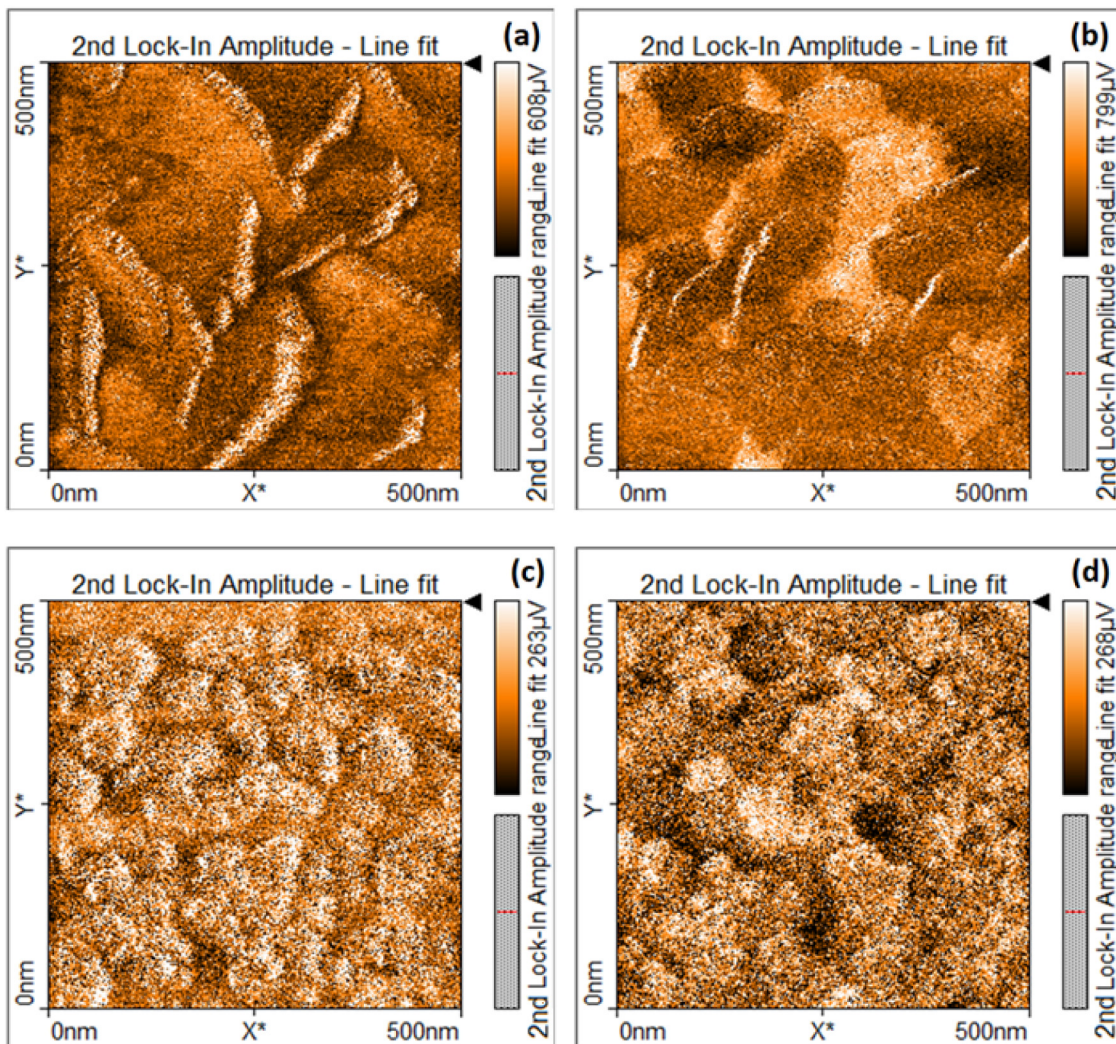
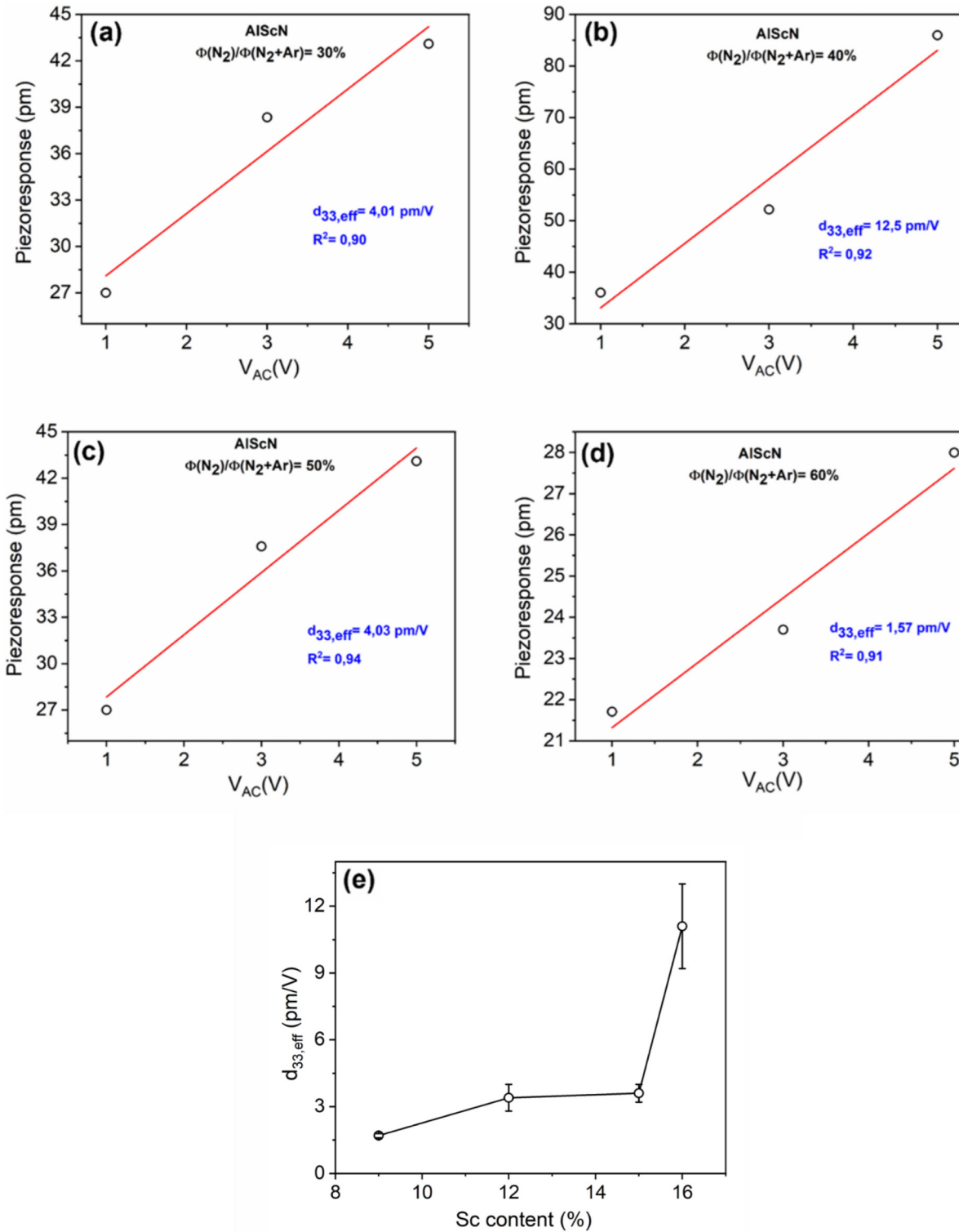


FIG. 6. Representative PFM piezo amplitude of $\text{Al}_{1-x}\text{Sc}_x\text{N}$ thin films at different N_2 flux percentage: (a) 30%, (b) 40%, (c) 50%, (d) 60% in the sputtering mixture recorded at 3 V of sinusoidal voltage.



10 December 2024 06:23:41

FIG. 7. Examples of displacement vs tip voltage to obtain the effective piezoelectric coefficient for $Al_{1-x}Sc_xN$ thin films at different N_2 flux percentage [(a)–(d)]; trend of the average piezo-response values ($d_{33,eff}$) of the investigated films obtained by PFM analysis (e).

TABLE IV. Surface potential of the analyzed films obtained by KPFM measurements.

Sample	Surface potential V_{CPD} (eV)	ϕ_{sample} (eV)	% O
AlScN_30	0.287	4.62 ± 0.02	7
AlScN_40	0.099	4.43 ± 0.02	4
AlScN_50	0.073	4.40 ± 0.01	3
AlScN_60	0.183	4.51 ± 0.03	5

60% of reactive gas percentage (or, similarly, with the lowest Sc content), which show smaller crystallite sizes and more agglomerates. These results are in good accordance with XRD analyses.

B. Piezoelectric responses of the $Al_{1-x}Sc_xN$ thin films: PFM and KPFM measurements

From chemical analysis, the sample labeled AlScN_40 is the film with the highest Sc content incorporation. From the structural point of view, it results in the best quality with an improved crystallite size growth. These results are in line with what experimentally found in terms of the piezoelectric response of $Al_{1-x}Sc_xN$ thin films.

Figure 6 reports the PFM amplitude maps of the samples, recorded by the second lock-in. The values of amplitude reported in Volt are strictly correlated to the deformation of the sample surface due to the piezoelectric effect. The higher the value of the applied voltage, the higher the strain will be, which is calculated in pm/V.

Figures 7(a)–7(d) show the displacement evaluated by a single measurement for each sample by varying the V_{AC} voltage applied to the tip between 1 and 5 V, obtaining the piezoelectric coefficient $d_{33,eff}$ from the linear regression. Figure 7(e) depicts the trend of $d_{33,eff}$ vs Sc content (i.e., the piezo-response) of the investigated

films; each $d_{33,eff}$ value (also reported in Table I) represents the average of ten different measurements.

The dependence of $d_{33,eff}$ on the Sc content in $Al_{1-x}Sc_xN$ thin films is a clear indication of changes in the wurtzite structure of nitride films, which is related to the tuning of the reactive gas concentration. In our experimental conditions, the reactive gas concentration equal to 40% represents the best value for an effective insertion of Sc atoms into the AlN wurtzite structure such to gain the highest piezoelectric coefficient $d_{33,eff}$ equal to 11.1 pm/V. The piezoelectric constant values follow the same trend of the crystallite size, reaching the highest value at the highest crystallite size (43.9 nm for AlScN_40), confirming the correlation between a more ordered structural arrangement of the film with an enhanced piezoelectric response. This can be also deduced from PFM amplitudes, which are more homogeneous for this sample, promoting the enhancement of the piezoelectric response. An additional consideration can be done by taking into account the results coming from chemical analysis (see Tables II and III). The more intense piezoelectric response of AlScN_40 sample can be attributable not only to the higher Sc atoms incorporation but also to the lower oxygen content. Indeed, the presence of oxygen in piezoelectric films is known to limit the performance of the final device.^{46,47} If we consider the different sources of contaminant as previously reported in the discussion, it can be deduced that the oxygen atoms incorporated into the only active films (AlScN layer) is lower than the total oxygen detected by the RBS technique. Furthermore, the film with the highest piezoelectric performance resulted in AlScN_40, where the lowest oxygen content was detected. These considerations are further supported by surface potential evaluation obtained by KPFM analysis (Table IV).

The highest surface potential values were measured for the AlScN_30 and AlScN_60 films: the higher oxygen content detected in these samples causes a more intense charging effect⁴⁸ compared to the less contaminated ones. All positive V_{CPD} values indicate

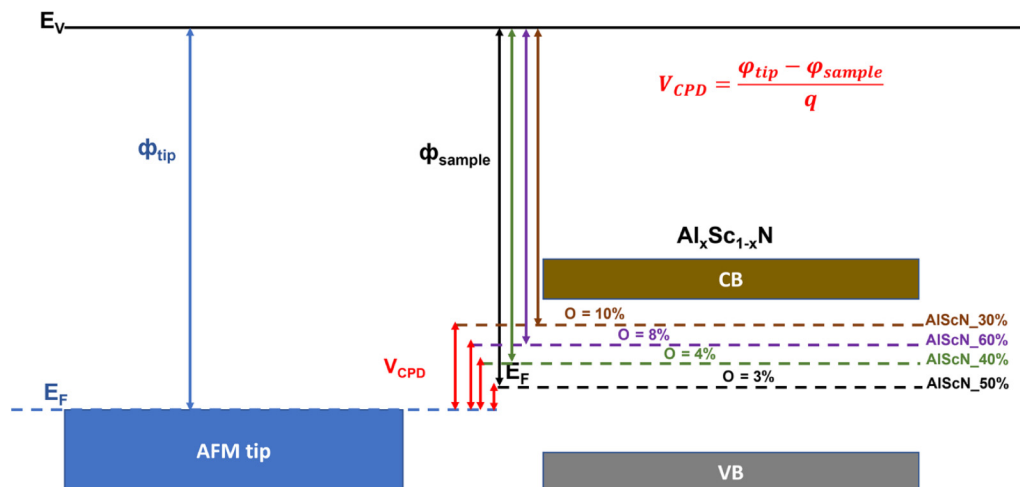


FIG. 8. Schematization of the variation of the work function of the investigated films with respect to the work function of the KPFM tip (E_F : fermi level, CB: conduction band, VB: valence band).

TABLE V. Comparison of d_{33} values reported in the literature for AlN and $\text{Al}_{1-x}\text{Sc}_x\text{N}$ with those obtained by our CNR research group (highlighted in bold).

Research group	AlN (pm/V)	$\text{Al}_{1-x}\text{Sc}_x\text{N}$ (pm/V)	x	% increment
Su <i>et al.</i> ¹⁴	...	9.3	0.27	...
Casamento <i>et al.</i> ¹⁹	6	15	0.18	150
Zukauskaitė <i>et al.</i> ²⁸	1.3	2.1	0.20	62
Mertin <i>et al.</i> ²⁹	4	7	0.18	75
Tang <i>et al.</i> ³⁰	7.1	13.7	0.15	93
Signore <i>et al.</i> ⁵⁰	3.7	11.1	0.16	200

that the work functions of all thin films (ϕ_{sample}) are lower than the work function of the AFM tip (ϕ_{tip}), considering the known relation⁴⁹

$$V_{\text{CPD}} = \frac{\phi_{\text{tip}} - \phi_{\text{sample}}}{q}. \quad (2)$$

Figure 8 depicts a simple schematic to clarify the variation of the $\text{Al}_{1-x}\text{Sc}_x\text{N}$ work function according to the deposition conditions and the oxygen content evaluated by RBS analysis. The shift of the nitride Fermi energy level (E_F) upward is justified by positive increasing V_{CPD} values, as depicted.

The evaluation of the surface potential of the films represents an important tool for the calculation of a purer piezoelectric response of the material. It is largely known that during the PFM measurement, an electrostatic contribution always occurs, due to the electrostatic force induced by the Coulomb interaction between separated charges of the AFM tip/cantilever and the sample surface.^{50,51} This contribution can be nullified by adding a DC bias voltage to the tip during PFM measurement so that the potential applied to the sample is $V_{\text{AC}} + V_{\text{DC}}$ and $V_{\text{DC}} = V_{\text{CPD}}$.^{50,52}

Following this procedure, the piezoelectric coefficient of the films was corrected by eliminating the electrostatic contribution, providing a final value equal to 8.9 pm/V for the AlScN_40 sample.

In general, all the piezoelectric coefficient values found in our experiments are consistent with the literature trend considering that the value of Sc concentration for our best result is lower than the optimal interval reported in literature to obtain higher piezoelectric response (up to 50%⁵³). As a matter of fact, in the range of Sc concentration between 10% and 20% in the AlN matrix, d_{33} expected values are lower than our experimental piezoelectric coefficients.

Table V shows a comparison between d_{33} values reported in the literature for AlN and $\text{Al}_{1-x}\text{Sc}_x\text{N}$.

It can be seen from Table V that our results rank among the best in the state of the art, achieving the greatest percentage increase in the performance of Sc-doped AlN film compared to the undoped one. These results become even more valuable when considering that the films were grown at low temperatures, with the consequent advantages previously mentioned in terms of MEMS fabrication and compatibility with CMOS technology.

IV. CONCLUSIONS

This work deals with the low-temperature deposition and characterization of $\text{Al}_{1-x}\text{Sc}_x\text{N}$ thin films realized by sputtering from AlSc alloy target on the Ti seed layer to promote the growth along c axis. The influence of N_2 concentration in the ($\text{Ar} + \text{N}_2$) sputtering atmosphere on the structural, morphological, chemical, and piezoelectric properties of the ternary compounds was studied. It is demonstrated that, in our experimental conditions, a good structural and morphological quality of wurtzite $\text{Al}_{1-x}\text{Sc}_x\text{N}$ thin film is obtained at N_2 concentration equal to 40%, exhibiting the most intense piezoelectric response. Specifically, d_{33} piezoelectric coefficient reaches the value of 11.1 pm/V, increasing up to 200% compared to the undoped film value (3.7 pm/V) thanks to Sc insertion into AlN wurtzite lattice. These results become even more valuable if compared to the state of the art, especially considering the film deposition at low temperature which generally does not favor the achievement of a very high structural quality necessary for improved piezoelectric properties.

It is remarkable to evidence that this work provides for the first time the d_{33} piezoelectric constant of $\text{Al}_{1-x}\text{Sc}_x\text{N}$ thin film cleared from electrostatic contribution through the evaluation of the surface potential by using the KPFM technique. The final value found for $\text{Al}_{1-x}\text{Sc}_x\text{N}$ thin film with $x = 0.16$ is 8.9 pm/V.

Future work will be devoted to further optimizing the growth process to achieve texture improvement, grain growth rising, Sc concentration increase, with the aim to enhance the piezoelectric response of this new material, which represents an attractive opportunity for high-performance piezoelectric device fabrication.

AUTHOR DECLARATIONS

Conflict of Interest

The authors have no conflicts to disclose.

Author Contributions

M. A. Signore: Conceptualization (lead); Data curation (lead); Investigation (lead); Methodology (lead); Supervision (lead); Validation (lead); Visualization (lead). **A. Serra:** Data curation (equal); Investigation (equal); Visualization (equal). **D. Manno:** Data curation (equal); Investigation (equal); Visualization (equal). **G. Quarta:** Investigation (equal); Methodology (equal); Visualization (equal). **L. Calcagnile:** Investigation (equal); Visualization (equal). **L. Maruccio:** Investigation (equal); Methodology (equal); Visualization (equal). **E. Sciurtti:** Investigation (equal); Visualization (equal). **E. Melissano:** Investigation (equal); Visualization (equal). **A. Campa:** Investigation (equal); Visualization (equal). **M. C. Martucci:** Investigation (equal); Visualization (equal). **L. Francioso:** Funding acquisition (lead); Validation (equal); Visualization (equal). **L. Velardi:** Conceptualization (lead); Data curation (lead); Investigation (lead); Methodology (lead); Supervision (lead); Validation (lead); Visualization (lead); Writing – original draft (lead); Writing – review & editing (lead).

DATA AVAILABILITY

The data that support the findings of this study are available from the corresponding author upon reasonable request.

REFERENCES

- ¹T. Li and P. S. Lee, "Piezoelectric energy harvesting technology: From materials, structures, to applications," *Small Struct.* **3**, 2100128 (2022).
- ²J. L. Edmunds, S. Sonmezoglu, J. Martens, A. Von Meier, and M. M. Maharbiz, "Optical voltage sensor based on a piezoelectric thin film for grid applications," *Opt. Express* **29**, 33716–33727 (2021).
- ³V. P. Elanjitsenni, K. S. Vadivu, and B. M. Prasanth, "A review on thin films, conducting polymers as sensor devices," *Mater. Res. Express* **9**, 022001 (2022).
- ⁴K. Ruotsalainen, D. Morits, O. M. E. Ylivaara, and J. Kynäräinen, "Resonating AlN-thin film MEMS mirror with digital control," *J. Opt. Microsyst.* **2**(1), 011006 (2022).
- ⁵M. A. Signore, A. Taurino, M. Catalano, M. Kim, Z. Che, F. Quaranta, and P. Siciliano, "Growth assessment of (002)-oriented AlN thin films on Ti bottom electrode deposited on silicon and Kapton substrates," *Mater. Design* **119**, 151–158 (2017).
- ⁶K. Hirata, Y. Mori, H. Yamada, M. Uehara, S. A. Anggraini, and M. Akiyama, "Significant enhancement of piezoelectric response in AlN by Yb addition," *Materials* **14**, 309 (2021).
- ⁷Y. Liu, L. Wang, Y. Su, Y. Zhang, Y. Wang, and Z. Wu, "AlScN piezoelectric MEMS mirrors with large field of view for LiDAR application," *Micromachines* **13**, 1550 (2022).
- ⁸C. Stoeckel, K. Meinel, M. Melzer, A. Žukauskaitė, S. Zimmermann, R. Forke, K. Hiller, and H. Kuhn, "Static high voltage actuation of piezoelectric AlN and AlScN based scanning micromirrors," *Micromachines* **13**, 625 (2022).
- ⁹J. Yan, Y. Zhou, and S. Zhang, "Development of high uniformity Al_{1-x}Sc_xN piezoelectric film stack dry etching process on 8-inch silicon wafers," *Vacuum* **210**, 111907 (2023).
- ¹⁰K. Men, H. Liu, X. Wang, Q. Jia, Z. Ding, H. Wu, D. Wu, and Y. Xiong, "AlScN films prepared by alloy targets and SAW device characteristics," *J. Rare Earths* **41**, 434 (2023).
- ¹¹Y. Lu, M. Reusch, N. Kurz, A. Ding, T. Christoph, L. Kirste, V. Lebedev, and A. Žukauskaitė, "Surface morphology and microstructure of pulsed DC magnetron sputtered piezoelectric AlN and AlScN thin films," *Phys. Status Solidi A* **215**, 1700559 (2018).
- ¹²S. Barth, H. Bartzsch, D. Glöß, P. Frach, T. Modes, O. Zywitzki, G. Suchanek, and G. Gerlach, "Magnetron sputtering of piezoelectric AlN and AlScN thin films and their use in energy harvesting applications," *Microsyst. Technol.* **22**, 1613–1617 (2016).
- ¹³D. Solonenko, A. Žukauskaitė, J. Pilz, M. Morigi, and S. Riguez, "Raman spectroscopy and spectral signatures of AlScN/Al₂O₃," *Micromachines (Basel)* **13**, 1961 (2022).
- ¹⁴J. Su, S. Fichtner, M. Z. Ghori, N. Wolff, M. R. Islam, A. Lotnyk, D. Kaden, F. Niekie, L. Kienle, B. Wagner, and F. Lofink, "Growth of highly c-axis oriented AlScN films on commercial substrates," *Micromachines* **13**, 783 (2022).
- ¹⁵S. Fichtner, T. Reimer, S. Chemnitz, F. Lofink, and B. Wagner, "Stress controlled pulsed direct current co-sputtered Al_{1-x}Sc_xN as piezoelectric phase for micromechanical sensor applications," *APL Mater.* **3**, 116102 (2015).
- ¹⁶M. Sinusiá Lozano, A. Pérez-Campos, M. Reusch, L. Kirste, T. Fuchs, A. Žukauskaitė, Z. Chen, and G. F. Iriarte, "Piezoelectric characterization of Sc_{0.26}Al_{0.74}N layers on Si (001) substrates," *Mater. Res. Express* **5**, 036407 (2018).
- ¹⁷P. Wang, D. A. Laleyan, A. Pandey, Y. Sun, and Z. Mi, "Molecular beam epitaxy and characterization of wurtzite Sc_xAl_{1-x}N," *Appl. Phys. Lett.* **116**, 151903 (2020).
- ¹⁸N. Kurz, Y. Lu, L. Kirste, M. Reusch, A. Žukauskaitė, V. Lebedev, and O. Ambacher, "Temperature dependence of the pyroelectric coefficient of AlScN thin films," *Phys. Status Solidi A* **215**, 1700831 (2018).
- ¹⁹J. Casamento, C. S. Chang, Y.-T. Shao, J. Wright, D. A. Muller, H. (G.) Xing, and D. Jena, "Structural and piezoelectric properties of ultra-thin Sc_xAl_{1-x}N films grown on GaN by molecular beam epitaxy," *Appl. Phys. Lett.* **117**, 112101 (2020).
- ²⁰S. Leone, J. Ligl, C. Manz, L. Kirste, T. Fuchs, H. Menner, M. Prescher, J. Wiegert, A. Žukauskaitė, R. Quay, and O. Ambacher, "Metal-organic chemical vapor deposition of aluminum scandium nitride," *Phys. Status Solidi RRL* **14**, 1900535 (2020).
- ²¹S. Cheemadan and M. C. S. Kumar, "Effect of substrate temperature and oxygen partial pressure on RF sputtered NiO thin films," *Mater. Res. Express* **5**, 046401 (2018).
- ²²N. Hegedüs, K. Balázs, and C. Balázs, "Silicon nitride and hydrogenated silicon nitride thin films: A review of fabrication methods and applications," *Materials* **14**, 5658 (2021).
- ²³M. Akiyama, T. Kamohara, K. Kano, A. Teshigahara, Y. Takeuchi, and N. Kawahara, "Enhancement of piezoelectric response in scandium aluminum nitride alloy thin films prepared by dual reactive cosputtering," *Adv. Mater.* **21**, 593–596 (2009).
- ²⁴Y. Lu, "Development and characterization of piezoelectric AlScN-based alloys for electroacoustic applications," dissertation (Universitätsbibliothek Freiburg, 2019).
- ²⁵C. L. Fei, X. L. Liu, B. P. Zhu, D. Li, X. F. Yang, Y. T. Yang, and Q. F. Zhou, "AlN piezoelectric thin films for energy harvesting and acoustic devices," *Nano Energy* **51**, 146–161 (2018).
- ²⁶Y. Liu, Y. Cai, Y. Zhang, A. Tovstopyat, S. Liu, and C. L. Sun, "Materials, design, and characteristics of bulk acoustic wave resonator: A review," *Micromachines* **11**, 630 (2020).
- ²⁷O. Zywitzki, T. Modes, S. Barth, H. Bartzsch, and P. Frach, "Effect of scandium content on structure and piezoelectric properties of AlScN films deposited by reactive pulse magnetron sputtering," *Surf. Coat. Technol.* **309**, 417 (2017).
- ²⁸A. Zukauskaitė, G. Wingqvist, J. Palisaitis, J. Jensen, P. O. Å. Persson, R. Matloub, P. Murali, Y. Kim, J. Birch, and L. Hultman, "Microstructure and dielectric properties of piezoelectric magnetron sputtered w-Sc_xAl_{1-x}N thin films," *J. Appl. Phys.* **111**, 093527 (2012).
- ²⁹S. Mertin, V. P. Pashchenko, F. Parsapour, C. S. Sandu, B. Heinz, O. Rattunde, G. Christmann, M. A. Dubois, and P. Murali, "Enhanced piezoelectric properties of c-axis textured aluminium scandium nitride thin films with high scandium content: Influence of intrinsic stress and sputtering parameters," *IEEE Int. Ultrason. Symp. (IUS)* 2017, 1.
- ³⁰J. Tang, D. Niu, Z. Tai, and X. Hu, "Deposition of highly c-axis-oriented ScAlN thin films at different sputtering power," *J. Mater. Sci. Mater. Electron.* **28**, 5512 (2017).
- ³¹J. Kiihamäki, H. Kattelus, M. Blomberg, R. Puurunen, M. Laamanen, P. Pekko, and A. Rissanen, "Low-temperature processes for MEMS device fabrication," in *Advanced Materials and Technologies for Micro/Nano-Devices, Sensors and Actuators. NATO Science for Peace and Security Series B Physics and Biophysics*, edited by E. Gusev, E. Garfunkel, and A. Dideikin (Springer, Dordrecht, 2010), pp. 167–178.
- ³²J. M. Wall and F. Yan, "Sputtering process of Sc_xAl_{1-x}N thin films for ferroelectric applications," *Coatings* **13**, 54 (2023).
- ³³L. Calcagnile, G. Quarta, M. D'Elia, D. Muscogiuri, L. Maruccio, K. Butalag, G. Gianfrate, C. Sanapo, and U. Toma, "Instrumental developments at the IBA-AMS dating facility at the University of Lecce," *Nucl. Instrum. Methods Phys. Res. Section B* **240**, 22–25 (2005).
- ³⁴B. D. Cullity and S. R. Stock, *Elements of X-Ray Diffraction*, 3rd ed. (Prentice-Hall, Englewood Cliffs, NJ, 2001).
- ³⁵L. Aissani, M. Fellah, A. H. Chadli, M. A. Samad, A. Cheriet, F. Salhi, C. Nouveau, S. Weiß, A. Obrosova, and A. Alhoussein, "Investigating the effect of nitrogen on the structural and tribo-mechanical behavior of vanadium nitride thin films deposited using R.F. Magnetron sputtering," *J. Mater. Sci.* **56**, 17319–17336 (2021).
- ³⁶L. Habl, D. Rafalskyi, and T. Lafleur, "Secondary electron emission due to multi-species iodine ion bombardment of different target materials," *J. Appl. Phys.* **129**, 153302 (2021).

- ³⁷F. Parsapour, V. Pashchenko, N. Kurz, C. S. Sandu, T. LaGrange, K. Yamashita, V. Lebedev, and P. Mural, "Material parameter extraction for complex AlScN thin film using dual mode resonators in combination with advanced microstructural analysis and finite element modeling," *Adv. Electron. Mater.* **5**, 1800776 (2019).
- ³⁸M. Sumisaka, K. Yamazaki, S. Fujii, G. Tang, T. Han, Y. Suzuki, S. Otomori, T. Omori, and K. Hashimoto, "Sputter deposition of ScAlN using large size alloy target with high Sc content and reduction of Sc content in deposited films," *Jpn. J. Appl. Phys.* **54**, 07HD06 (2015).
- ³⁹Y.-P. Chien, S. Mráz, M. Fekete, M. Hans, D. Primetzhofer, S. Kolozsvári, P. Polcik, and J. M. Schneider, "Deviations between film and target compositions induced by backscattered Ar during sputtering from M2-Al-C (M = Cr, Zr, and Hf) composite targets," *Surf. Coat. Technol.* **446**, 128764 (2022).
- ⁴⁰S. Mertin, B. Heinz, O. Rattunde, G. Christmann, M. A. Dubois, S. Nicolay, and P. Mural, "Piezoelectric and structural properties of c-axis textured aluminum scandium nitride thin films up to high scandium content," *Surf. Coat. Technol.* **343**, 2–6 (2018).
- ⁴¹W. J. Liauh, S. Wu, J. L. Huang, D. F. Lii, Z. X. Lin, and W. K. Yeh, "Microstructure and piezoelectric properties of reactively sputtered highly C-axis $\text{Sc}_x\text{Al}_{1-x}\text{N}$ thin films on diamond-like carbon/Si substrate," *Surf. Coat. Technol.* **308**, 101 (2016).
- ⁴²P. M. Mayrhofer, C. Eisenmenger-Sittner, M. Stöger-Pollach, H. Euchner, A. Bittner, and U. Schmid, "The impact of argon admixture on the c-axis oriented growth of direct current magnetron sputtered $\text{Sc}_x\text{Al}_{1-x}\text{N}$ thin films," *J. Appl. Phys.* **115**, 193505 (2014).
- ⁴³G. Schönweger, A. Petraru, M. R. Islam, N. Wolff, B. Haas, A. Hammud, C. Koch, L. Kienle, H. Kohlstedt, and S. Fichtner, "From fully strained to relaxed: Epitaxial ferroelectric $\text{Al}_{1-x}\text{Sc}_x\text{N}$ for III-N technology," *Adv. Funct. Mater.* **32**, 2109632 (2022).
- ⁴⁴S. Satoh, K. Ohtaka, T. Shimatsu, and S. Tanaka, "Crystal structure deformation and phase transition of AlScN thin films in whole Sc concentration range," *J. Appl. Phys.* **132**, 025103 (2022).
- ⁴⁵C. Höglund, J. Birch, B. Alling, J. Bareño, Z. Czigány, P. O. Å. Persson, G. Wingqvist, A. Zukauskaitė, and L. Hultman, "Wurtzite structure $\text{Sc}_{1-x}\text{Al}_x\text{N}$ solid solution films grown by reactive magnetron sputter epitaxy: Structural characterization and first-principles calculations," *J. Appl. Phys.* **107**, 123515 (2010).
- ⁴⁶G. Schönweger, M. R. Islam, N. Wolff, A. Petraru, L. Kienle, H. Kohlstedt, and S. Fichtner, "Ultrathin $\text{Al}_{1-x}\text{Sc}_x\text{N}$ for low-voltage-driven ferroelectric-based devices," *Phys. Status Solidi RRL* **17**, 2200312 (2023).
- ⁴⁷P. Döring, S. Krause, P. Waltereit, P. Brückner, S. Leone, I. Streicher, M. Mikulla, and R. Quay, "Voltage-margin limiting mechanisms of AlScN-based HEMTs," *Appl. Phys. Lett.* **123**, 032101 (2023).
- ⁴⁸Q. Wang, X. Liang, K. Chen, C. Wu, and S. Liu, "Surface charge properties of epoxy composites under DC voltage affected by surface and bulk conductivity," *Energies* **14**, 370 (2021).
- ⁴⁹M. DeJarld, P. M. Campbell, A. L. Friedman, M. Currie, R. L. Myers-Ward, A. K. Boyd, S. G. Rosenberg, S. P. Pavunny, K. M. Daniels, and D. K. Gaskill, "Surface potential and thin film quality of low work function metals on epitaxial graphene," *Sci. Rep.* **8**, 16487 (2018).
- ⁵⁰M. A. Signore, L. Francioso, C. De Pascali, A. Serra, D. Manno, G. Rescio, F. Quaranta, E. Melissano, and L. Velardi, "Improvement of the piezoelectric response of AlN thin films through the evaluation of the contact surface potential by piezoresponse force microscopy," *Vacuum* **218**, 112596 (2023).
- ⁵¹B. J. Rodriguez, C. Callahan, S. V. Kalinin, and R. Proksch, "Dual-frequency resonance-tracking atomic force microscopy," *Nanotechnology* **18**, 475504 (2007).
- ⁵²D. Seol, S. Kang, C. Sun, and Y. Kim, "Significance of electrostatic interactions due to surface potential in piezoresponse force microscopy," *Ultramicroscopy* **207**, 112839 (2019).
- ⁵³C. Höglund, J. Bareño, J. Birch, B. Alling, Z. Czigány, and L. Hultman, "Cubic $\text{Sc}_{1-x}\text{Al}_x\text{N}$ solid solution thin films deposited by reactive magnetron sputter epitaxy onto ScN(111)," *J. Appl. Phys.* **105**, 113517 (2009).